Opto-Electronic Advances

Supplementary information

March 2025, Vol. 8, No. 3

DOI: 10.29026/oea.2025.240182 CSTR: 32247.14.oea.2025.240182

Single-beam optical trap-based surface-enhanced raman scattering optofluidic molecular fingerprint spectroscopy detection system

Ning Sun, Yuan Gan, Yujie Wu, Xing Wang, Shen Shen, Yong Zhu and Jie Zhang*

The Key Laboratory of Optoelectronic Technology & System, Education Ministry of China, Chongqing University, Chongqing 400044, China.
*Correspondence: J Zhang, E-mail: zhangjie@cqu.edu.cn

This file includes:

Section 1: Experimental instrument materials and related parameters
Section 2: Preparation of tapered optical fiber
Section 3: Preparation of optofluidic chip
Section 4: Preparation of silver nanoparticles
Section 5: Calculation method of light scattering force and light gradient force
Section 6: Selection of optical tweezers parameters and comparison between tapered and ordinary optical fibers
Section 7: COMSOL simulation parameter settings
Section 8: Effect of AgNPs spacing on electric field intensity and Raman signal enhancement

Supplementary information for this paper is available at https://doi.org/10.29026/oea.2025.240182

Section 1: Experimental instrument materials and related parameters

Experimental material:Ascorbic acid (AA, $C_6H_8O_6 \geq 99.7\%$), silver nitrate ($AgNO_3 \geq 99.8\%$), sodium chloride ($NaCl \geq 99.5\%$), polyvinylpyrrolidone (PVP, $(C_6H_9NO)n$, excellent purity), ethyl alcohol(C_2H_6O) , sodium hydroxide ($NaOH \geq 96\%$), all of which were purchased from Aladin Chemical Reagent Co., LTD. Ultrapure water (18.2 MΩcm) produced by Millipore Milli-Q Advantage A10 water purification system. Dow Corning SYLGARD 184 Silicon elastomer (PDMS precursor and hardener).

Experimental instrument: 1550 nm Laser(We utilize a 1550 nm distributed feedback (DFB) laser characterized by a narrow linewidth, high side-mode suppression ratio (SMSR), and minimal temperature drift. However, standard DFB lasers typically struggle to achieve the 200 mW capture power required for our experiment. To address this issue, we introduced an erbium-doped fiber amplifier (EDFA) as a power enhancement solution. The incorporation of the EDFA effectively boosts the laser signal's power level to meet the detection system's demands. 532 nm Raman Spectrometer (A solid-state laser with a wavelength of 532 nm serves as the excitation light source, illuminating the sample under test. The scattering collection system includes a collimating lens, mirrors, and a focusing lens, which are used to collimate and focus the excitation beam onto the sample, guide the excitation beam to the sample, and collect and focus the Raman scattered light generated by the sample, respectively. The filtering system uses a long-pass filter to remove the excitation light, allowing only the Raman scattered light to pass through, thereby enhancing the signal-to-noise ratio. Within the spectrometer, a diffraction grating disperses the Raman scattered light according to its wavelength, and an imaging lens focuses the dispersed light onto a CCD detector, ensuring high spectral resolution. The detection system employs the CCD detector to convert the dispersed light signals into electrical signals. The signal processing circuit amplifies, filters, and digitizes these electrical signals using amplifiers, filters, and analog-to-digital converters. The data analysis and display system processes and presents the spectral data through a computer and software, displaying the results in the form of graphs and numerical data. The entire instrument is powered and managed by a power supply and control system, ensuring the efficient operation and accurate measurement of each component. These components work together to achieve high-sensitivity and high-resolution Raman spectroscopy measurement and analysis.), Plasma Cleaner, Vacuum Drying Oven, Magnetic Stirrer, Centrifuge, and Ultrasonic Cleaner. The AgNPs substrate was characterized using field emission electron microscope (FESEM, Thermo Scientific, Quattro S). Raman spectra were collected using a France HORIBA laser confocal Raman spectrometer equipped with a green Nd: yag 532 nm excitation laser. Raman test light source is 532 nm laser, power is 25 mW, integration time is 5 seconds, the objective lens selected 50 times telephoto. The spectral data in this paper are the results of multiple measurements averaged.

Section 2: Preparation of tapered optical fiber

We taper a 50-micron diameter multimode optical fiber to a taper tip of 25 microns. The process is as follows: First, prepare the fiber tapering furnace and stretching device. After cleaning the fiber, place it in the furnace and heat it with hydrogen generated by a hydrogen generator to the appropriate softening temperature, typically between 1000 °C and 2000 °C. Once heated, the fiber becomes pliable, and the stretching device is used to slowly draw the fiber, reducing its diameter from 50 microns to a taper tip of 25 microns. During this process, it is crucial to precisely control the speed and temperature to ensure the fiber forms a uniform taper. After tapering, allow the fiber to cool slowly to maintain its tapered structure. Finally, use a microscope to inspect and test the fiber, ensuring its diameter and shape meet the requirements, and perform any necessary post-processing. The fiber is then spliced with a pigtail (FC/APC) and connected to a laser through a connector. Figure S1(a) and S1(b) show optical photographs of the tapered fiber inspected using a microscope.

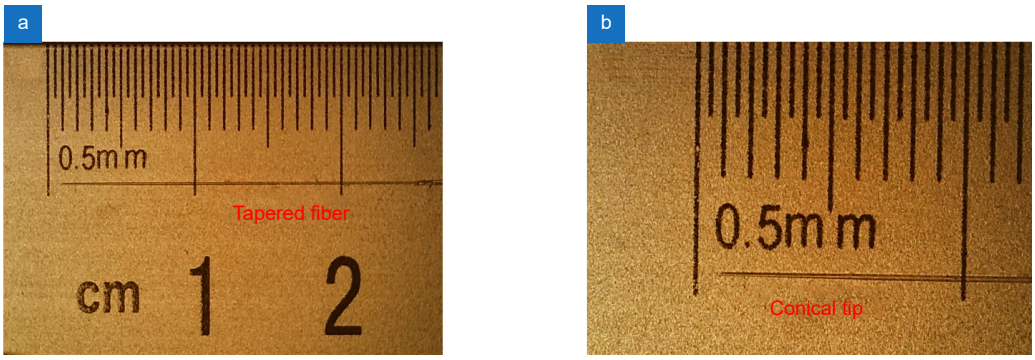

Fig. S1 | (**a**) and (**b**) show optical photographs of the 25-micron tapered fiber.

Section 3: Preparation of optofluidic chip

Begin by preparing the chip template using soft lithography techniques as follows: 1) Spin-coat SU-8 photoresist onto a smooth silicon wafer at 1250 rpm and bake it for 30 minutes. 2) After baking, place the designed mask on the coated silicon wafer and expose it to a 20 mW mercury lamp for 10 minutes. 3) Following exposure, heat the sample for an additional 15 minutes, then immerse the template in a developer solution for 10 minutes and rinse with the developer solution. 4) After rinsing, treat the template with trimethylchlorosilane for 30 minutes to achieve silanization, thus completing the preparation of the microchannel mold. This mold can be reused. Next, clean the glass slides and glass rod by washing them with anhydrous ethanol, rinsing with deionized water, and then drying them in either a natural environment or a vacuum drying oven. Gradually add the PDMS precursor to a container until the total mass reaches 20 grams, then add the curing agent until the total mass reaches 2 grams. Ensure the mass ratio of PDMS precursor to curing agent is 10∶1 for optimal curing. Stir the mixture thoroughly with a glass rod for 30 minutes to ensure uniform mixing. Place the mixture in a vacuum environment (such as a vacuum chamber) for 20 minutes to remove any bubbles. Cure the mixture at 70 °C in a vacuum drying oven for 240 minutes. After curing, allow the PDMS to cool, then separate the silicon mold from the PDMS to obtain the PDMS replica. Use a puncher to create inlet and outlet holes in the PDMS replica, and clean it with ethanol and deionized water to ensure cleanliness. Finally, place the PDMS replica with the channel side up on a clean glass slide, along with another clean glass slide, in a cleaner. Position the other PDMS replica with the channel side down on the glass slide and perform plasma-assisted bonding.

The optofluidic module used in this experiment includes input channels, transmission channels, a mixing region, a detection region, and output channels. The porous input channels allow the simultaneous introduction of analyte molecules and AgNPs, which remain unmixed due to the laminar flow effect. To achieve effective mixing, the module features a mixing region that converts laminar flow to turbulent flow, thereby enhancing the interaction between the components. The mixed fluid then enters the detection region, where it is uniformly irradiated by a laser beam, enabling highly sensitive Raman detection. Finally, the fluid is expelled through the output channels, completing the optofluidic process.

Section 4: Preparation of silver nanoparticles

Silver nanoparticles (AgNPs) with a diameter of 50 nm were prepared through a one-step reduction reaction and self-assembly method. Initially, solid $AgNO_3$ was introduced into a NaCl solution, followed by the addition of polyvinylpyrrolidone (PVP), resulting in a colloidal solution with AgCl as the precursor. In the subsequent step, under alkaline conditions, these precursors reacted with ascorbic acid (AA) to generate a colloidal solution of nano-silver. The detailed procedure and quantities used are as follows: First, 170 mg of PVP was added to 40 mL of ultrapure water, then 170 mg of solid $AgNO_3$ was incorporated, with constant magnetic stirring to ensure complete dissolution of the solids. Next, 400 μL of 5 mol/L NaCl solution was introduced to the mixture, which was further stirred for 15 minutes at room temperature and in darkness, yielding an AgCl colloidal solution. Thereafter, while maintaining agitation, 20 mL of 50 mmol/L AA was added to 2.5 mL of 0.5 mol/L NaOH solution. Following this, 2.5 mL of the AgCl colloidal solution

from the previous step was introduced and stirred for 2 hours under the same ambient and dark conditions, leading to the formation of AgNPs with a 50 nm diameter. Lastly, the obtained silver nanoparticle colloidal solution was centrifuged at 5000 rpm for 45 minutes, followed by ultrasonic dispersion in an ultrasonic disintegrator for 30 minutes. This final set of steps was repeated five times to eliminate residuals such as PVP. Figure S2(a) presents the SEM image of the prepared AgNPs, and Fig. S2(b) shows the statistical results of the AgNPs from (a), revealing an average particle diameter of approximately 50 nm. This is in line with the requirements for optical trapping.

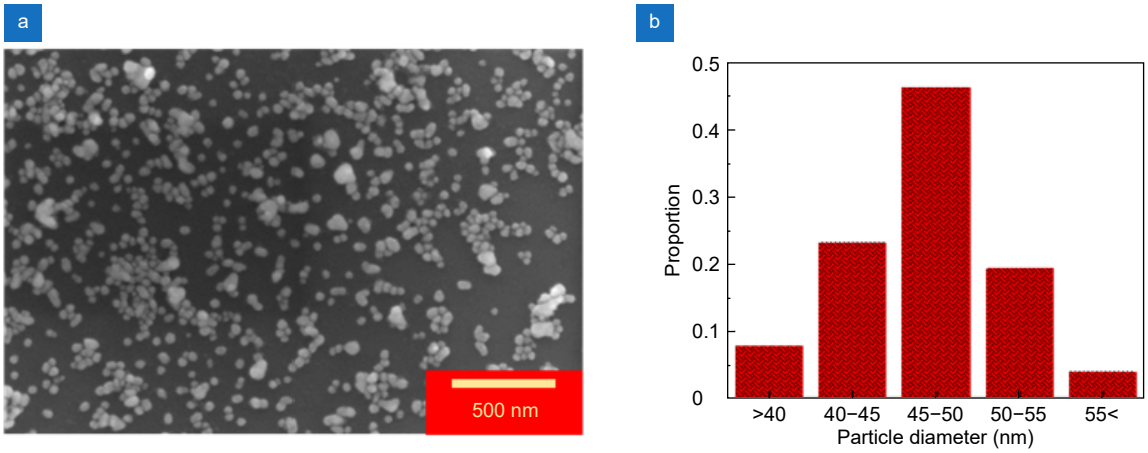

Fig. S2 | (**a**) SEM image of AgNPs. (**b**) statistical results of the AgNPs from (**a**).

The selection of AgNPs size in this study was made after careful consideration of multiple factors to ensure the accuracy of the experimental results, the stability of the system, and the scalability of the platform. The optimization process focused on the following key aspects:

1. Choice of laser wavelength for Raman testing: The enhancement of the Raman scattering effect is closely related to the localized surface plasmon resonance (LSPR) effect of the nanomaterials. To maximize this effect, we selected a laser with a wavelength of 532 nm as the excitation source for Raman testing. The 532 nm wavelength is a well-established and widely used option in Raman spectroscopy because the LSPR absorption peak of AgNPs is located near this wavelength. At this range, AgNPs can effectively absorb the laser energy and produce a strong LSPR effect, significantly enhancing the Raman signal. This enhancement not only improves detection sensitivity but also ensures the stability and consistency of the signal throughout the experiment. Therefore, the choice of the 532 nm laser is based on the absorption characteristics of AgNPs and its optimal compatibility with Raman testing.

2. Selection of laser wavelength for optical trapping: In the single-beam optical trap experiments, the choice of laser wavelength for trapping AgNPs is crucial. Based on the working principles of optical trapping and Rayleigh scattering theory, we employed a laser with a wavelength of 1550 nm for trapping. This wavelength is also commonly used and well-established in optical trapping experiments. In optical trapping systems, smaller nanoparticles exhibit higher trapping efficiency compared to larger particles because, at the nanoscale, the optical forces depend heavily on the particle's volume and refractive index. Smaller particles respond more effectively to the trapping laser, improving the stability and precision of the trapping process. Therefore, we prioritized smaller AgNPs to ensure the smooth execution of the trapping experiments.

3. Optimization of particle size and preparation method: To ensure experimental effectiveness while enhancing platform scalability and reducing system cost, we opted for the spontaneous nucleation method to synthesize AgNPs. This method is relatively simple, cost-effective, and suitable for large-scale production. When selecting particle size, we conducted a detailed comparative analysis of AgNPs with different diameters and ultimately chose AgNPs with a diameter of approximately 45–50 nm. This decision was based on the following considerations: (1) Size uniformity: experimental observations revealed that AgNPs with a diameter of 45–50 nm exhibited excellent size uniformity during synthesis, which is critical for consistent Raman detection results. Uniform particle size generates stable and reproducible hotspots, thereby enhancing the reliability of the Raman signal. (2) Oxidation resistance: compared to smaller AgNPs

(~20 nm in diameter), the relatively larger size (45–50 nm) of these particles reduces the likelihood of oxidation, allowing them to maintain their surface-enhanced Raman scattering (SERS) activity for longer periods. At the nanoscale, smaller particles have a higher surface area-to-volume ratio, making them more prone to react with oxygen in the air, which can quickly reduce their SERS activity. The selection of slightly larger particles helps extend the lifespan of AgNPs' activity, thus improving experimental stability and longevity. (3) Preparation efficiency: AgNPs with a diameter of 45–50 nm, compared to larger particles (~80 nm), yield a greater number of nanoparticles under the same reagent usage during synthesis (A silver nanosphere with a diameter of 80 nanometers contains approximately 1.572×10^8 silver atoms, and a silver nanosphere with a diameter of 50 nanometers contains approximately 3.833×10^6 silver atoms). This not only lowers preparation costs but also increases the density of hotspots in the experiment, thereby enhancing the detection efficiency of the entire system. The number of hotspots directly impacts the amplification effect of the Raman signal-more hotspots lead to stronger signal enhancement. Additionally, larger AgNPs tend to aggregate and deposit more easily during trapping, which can affect experimental stability, whereas particles around 50 nm show better dispersion under experimental conditions, reducing the risk of aggregation. In summary, the 45–50 nm AgNPs exhibited optimal performance within our experimental framework. On one hand, their moderate size balances effective optical trapping with a strong LSPR effect while minimizing oxidation and aggregation risks. On the other hand, their synthesis process is mature, providing high uniformity and scalability, reducing system complexity and cost. Therefore, the 45–50 nm AgNPs represent the optimal choice in our experimental system, providing a robust foundation for achieving efficient and stable SERS detection.

Section 5: Calculation method of light scattering force and light gradient force

The radius of the AgNPs we use is much smaller than the wavelength of the 1550 nm incident light commonly used in optical tweezers. Therefore, we can adopt the electromagnetic wave model based on Rayleigh scattering approximation. In this case, the AgNPs can be considered as point dipoles. When the particles are subjected to an electric field E, an induced electric dipole moment p is generated, with a magnitude given by:

$$\boldsymbol{p} = \alpha \boldsymbol{E} \,. \tag{S1}$$

The parameter α in the formula represents the polarizability, and its calculation formula is given by:

$$\alpha = 3V\varepsilon_0 \frac{\varepsilon_{\rm Ag} - \varepsilon_{\rm water}}{\varepsilon_{\rm Ag} + 2\varepsilon_{\rm water}} \,. \tag{S2}$$

In the formula, V represents the volume of the nanosphere, $V=3/4\pi R^3$, R is the radius of the particle, which is 25 nm. ε_0 represents the dielectric constant of vacuum, $\varepsilon_{\rm Ag}$ represents the dielectric constant of AgNPs, and $\varepsilon_{\rm water}$ represents the dielectric constant of the surrounding medium, which is water. The radiated power $P_{\rm scat}$ of an electric dipole can be expressed using the following formula:

$$P_{\rm scat} = \frac{k^4 |\boldsymbol{p}|}{6\pi\varepsilon_0 c^3} \,. \tag{S3}$$

$k=2\pi/\lambda$ is the wave number of the incident laser and c is the speed of light. The calculation formula of light intensity I is:

$$I = \frac{1}{2}\varepsilon_0 c|\boldsymbol{E}|^2 \,. \tag{S4}$$

Further, the scattering cross section of AgNPs can be calculated, and the scattering cross section $C_{\rm scat}$ is defined as:

$$C_{\rm scat} = \frac{P_{\rm scat}}{I} = \frac{k^4 |\alpha \boldsymbol{E}|}{6\pi\varepsilon_0 c^3 I} = \frac{8\pi^3 R^6}{\lambda^4} \left| \frac{\varepsilon_{\rm Ag} - \varepsilon_{\rm water}}{\varepsilon_{\rm Ag} + 2\varepsilon_{\rm water}} \right|^2 \,. \tag{S5}$$

The scattering force arises from the change in photon momentum. The total scattering force experienced by the particle is:

$$F_{\rm scat} = \frac{IC_{\rm scat}}{c} = \frac{8I\pi^3 R^6}{\lambda^4 c} \left| \frac{\varepsilon_{\rm Ag} - \varepsilon_{\rm water}}{\varepsilon_{\rm Ag} + 2\varepsilon_{\rm water}} \right|^2 \,. \tag{S6}$$

The force experienced by a particle in a non-uniform electric field can be described using the potential energy. The potential energy U of the particle in the electric field can be expressed as:

$$U = -\frac{1}{2}\boldsymbol{p}\cdot\boldsymbol{E} = -\frac{1}{2}\alpha|\boldsymbol{E}|^2 . \tag{S7}$$

The force F_{grad} experienced by the particle is the gradient of the potential energy with respect to the spatial coordinates:

$$F_{\text{grad}} = -\nabla U = -\left(-\frac{1}{2}\alpha|\boldsymbol{E}|^2\right) = \frac{1}{2}\alpha\nabla|\boldsymbol{E}|^2 . \tag{S8}$$

The particle will experience a force directed towards the region of increasing electric field strength. This is because, in a non-uniform electric field, polarized particles are attracted to areas of stronger electric fields in order to reach a state of lower energy. Since the polarizability of AgNPs is a complex number, the real part needs to be considered:

$$F_{\text{grad}} = -\frac{1}{2}\text{Re}(\alpha)\nabla|\boldsymbol{E}|^2 . \tag{S9}$$

Section 6: Selection of optical tweezers parameters and comparison between tapered and ordinary optical fibers

We chose the wavelength of 1550 nm because it generates a more effective light field gradient at the tip of the tapered fiber, significantly enhancing the optical trapping force[S1-S3]. This facilitates easier aggregation of nanoparticles and maintains stability in the capture area. Additionally, this enhancement effect reduces capture time and lowers the demand for high-power lasers. Furthermore, the 1550 nm laser exhibits lower energy loss in the experimental environment, greatly improving the optical system's transmission efficiency, which is another reason for its superior performance in this experiment.

Figure S3 is a simulation diagram of the optical field of a Gaussian beam propagating through a tapered optical fiber into water. Figure S3(a–d) show regular optical fibers with diameters of 50 microns, 25 microns, and 5 microns, and a tapered optical fiber (with a tapered tip diameter of 25 microns and an end diameter of 50 microns, drawn from a 50-micron optical fiber). By comparing Fig. S3(a1, a2, b1, b2, and c1, c2), we find that with an input power of 200 mW, the larger the fiber diameter, the lower the intensity of the optical field. Additionally, the position of the maximum optical field intensity is farther from the fiber end, and the spot size is larger. In Fig. S3(d1, d2, and d3), we observe that the tapered optical fiber can simulate an optical field with a high convergence angle. These differences mainly arise from the inclined surface of the fiber, which allows the beam to achieve a larger convergence angle. However, the inclined surface of the fiber also exhibits a mode leakage effect, where some light leaks out during refraction and reflection, leading to a specific optical field distribution. The characteristic of this optical field is that it forms a very small region at the tip of the tapered optical fiber where the optical field intensity reaches its maximum value. This design enables us to precisely capture AgNPs within the high-intensity optical field region, significantly reducing the spacing between the AgNPs.

Using Matlab simulations, we found that the tapered optical fiber can simulate an optical field with a high convergence angle. The characteristic of this optical field is that it forms a very small region at the tip of the tapered optical fiber where the optical field intensity reaches its maximum value. This design allows us to precisely position AgNPs within this high-intensity optical field region, significantly reducing the spacing between AgNPs. We simulated the trapping effects of optical fibers with different diameters and particularly focused on the differences between tapered optical fibers and traditional optical fibers. These differences mainly arise from the mode leakage effect on the inclined surface of the fiber, where some light leaks out during refraction and reflection on the inclined surface, forming a specific optical field distribution. Ultimately, combining the simulations with experimental findings, we discovered that the tapered optical fiber with a tip diameter of 25 microns, as shown in Fig. S3(d1, d2, and d3), best meets our requirements.

To gain a deeper understanding of the relationship between laser power and trapping performance, we conducted an analysis of the effects of laser power on the forces acting on particles through Matlab simulations. The results revealed that as laser power increased from 100 mW to 300 mW (Fig. S4(a1–c1)), the total force on the particles correspondingly rose (Fig. S4(a2–c2)). Increased laser power significantly enhances the trapping force, facilitating particle aggregation

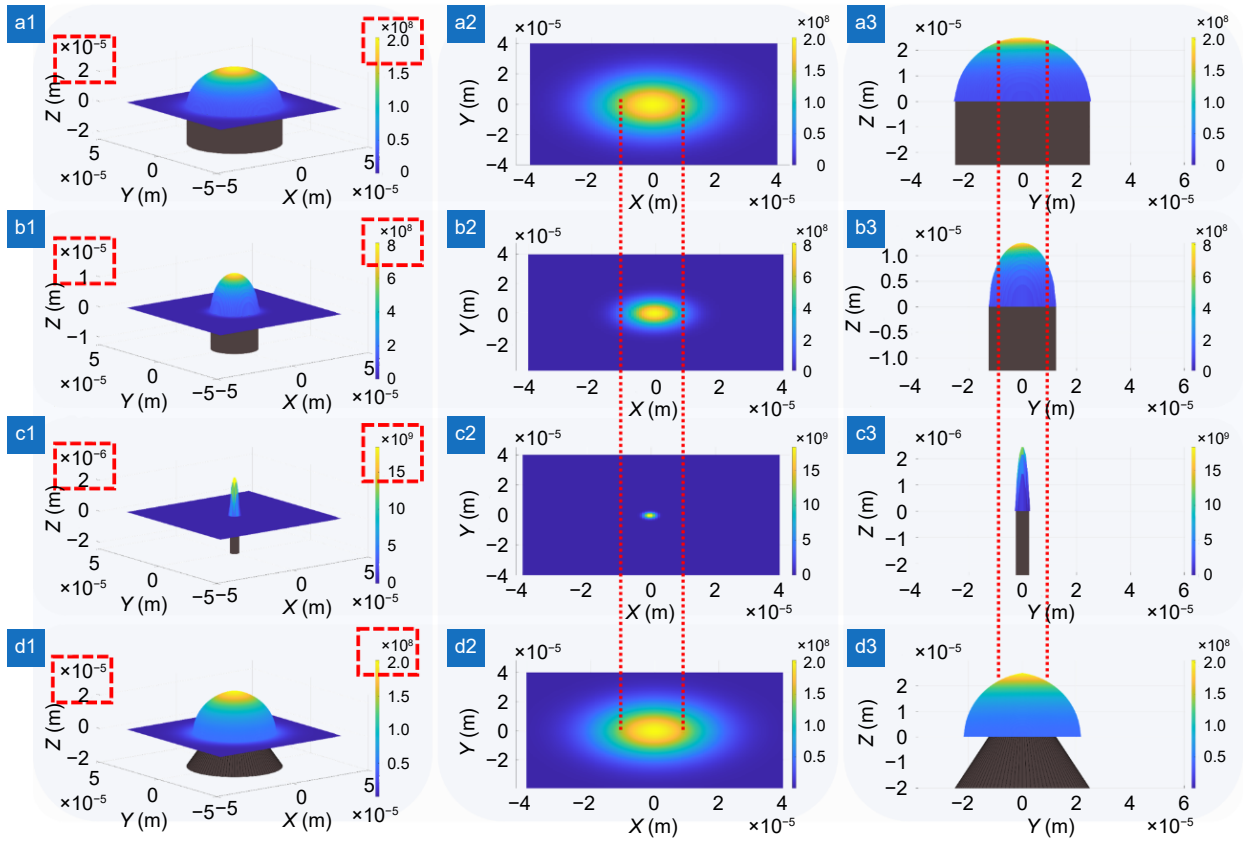

Fig. S3 | (**a1**, **a2**, **a3**) Show the three-dimensional optical field diagram, top view, and side view of a regular optical fiber with a diameter of 50 μm simulated using MATLAB. (**b1**, **b2**, **b3**) Respectively display the three-dimensional image, top view, and side view of the optical field for a regular optical fiber with a diameter of 25 μm. (**c1**, **c2**, **c3**) Respectively present the three-dimensional image, top view, and side view of the optical field for a regular optical fiber with a diameter of 5 μm. (**d1**, **d2**, **d3**) The three-dimensional images, top view, and side view of the optical field for a tapered optical fiber (with a tapered tip diameter of 25 μm and an end diameter of 50 μm, drawn from a 50 μm optical fiber).

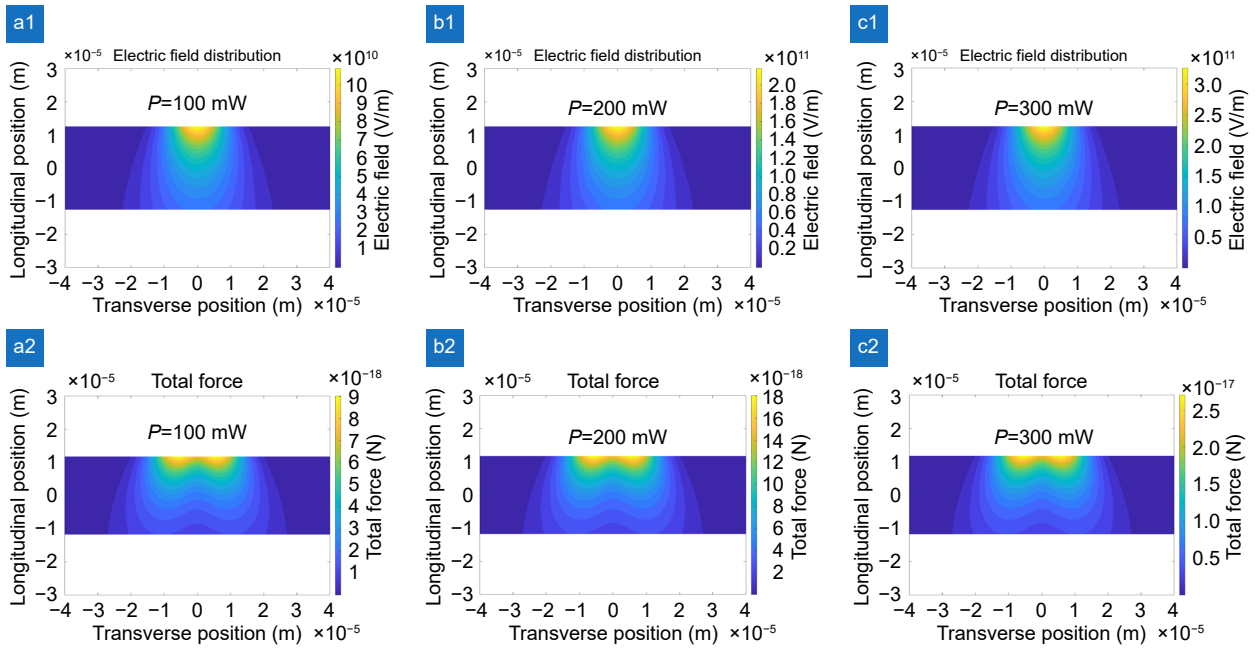

Fig. S4 | (**a1**) Electric field distribution at a laser power of 100 mW. (**a2**) Total force on the particles at a laser power of 100 mW. (**b1**) Electric field distribution at a laser power of 200 mW. (**b2**) Total force on the particles at a laser power of 200 mW. (**c1**) Electric field distribution at a laser power of 300 mW. (**c2**) Total force on the particles at a laser power of 300 mW.

and immobilization in the optical trap, which in turn improves trapping efficiency and aggregation quality. However, higher laser power also requires more expensive power amplification devices to maintain stable high output, resulting in increased overall system costs. To strike a balance between performance and cost, we plan to enhance the trapping circuit design in future studies to improve power efficiency. Our goal is to achieve better trapping performance without a significant rise in costs. By optimizing the system's power management and optical path design, we aim to further enhance trapping efficiency and signal quality, ultimately enabling broader application scenarios. Corresponding modifications have been updated on page 11 of the SI.

Section 7: COMSOL simulation parameter settings

To study the mechanism of constructing a high-gradient optical field with a tapered optical fiber, we established a simulation model using COMSOL Multiphysics. In this model, the wavelength of the incident light source is set to 1550 nm, the incident mode propagates along the *z*-direction, and the power of the incident light source is set to 200 mW. We assume the excitation wavelength is 532 nm and set the refractive indices of the optical fiber and water (H_2O) to 1.5 and 1.3350 [S4], respectively. The tapered tip diameter of the optical fiber is set to 4 μm, and the total length of the fiber is set to 9 μm.

In the AgNPs model, the wavelength of the incident light source was set to 532 nm, the incident mode was directed in the *z*-direction, and the incident electric field intensity was set to 1 V/m. We considered the excitation wavelength λ=532 nm and set the refractive indices for H_2O and AgNPs as follows: 0.13302+3.0284i[S5], 1.3350. Based on SEM characterization results, the diameter of AgNPs was 50 nm.

Section 8: Effect of AgNPs spacing on electric field intensity and Raman signal enhancement

We demonstrate the corresponding relationship between decreasing AgNPs spacing, increasing electric field intensity, and the gradual enhancement of the Raman signal in a single-beam optical trap.

Figure S5(a) shows the electric field simulation model of 50 nm diameter AgNPs under 532 nm laser excitation with varying gaps. Figure S5(b) presents the Raman line mapping positions. Figure S5(c1) illustrates the electric field distribution when the gap is 1 nm at position 7, while Fig. S5(c2) shows the Raman characteristic peak intensity of CV (10^{-6} mol/L) at 913 cm^{-1} at the same position. Figure S5(d1) displays the electric field distribution for a 5 nm gap at position 9, with the corresponding Raman characteristic peak intensity at 913 cm^{-1} shown in Fig. S5(d2). Finally, Fig. S5(e1) depicts the electric field distribution for a 9 nm gap at position 11, and Fig. S5(e2) shows the associated Raman peak intensity at 913 cm^{-1} at the same position.

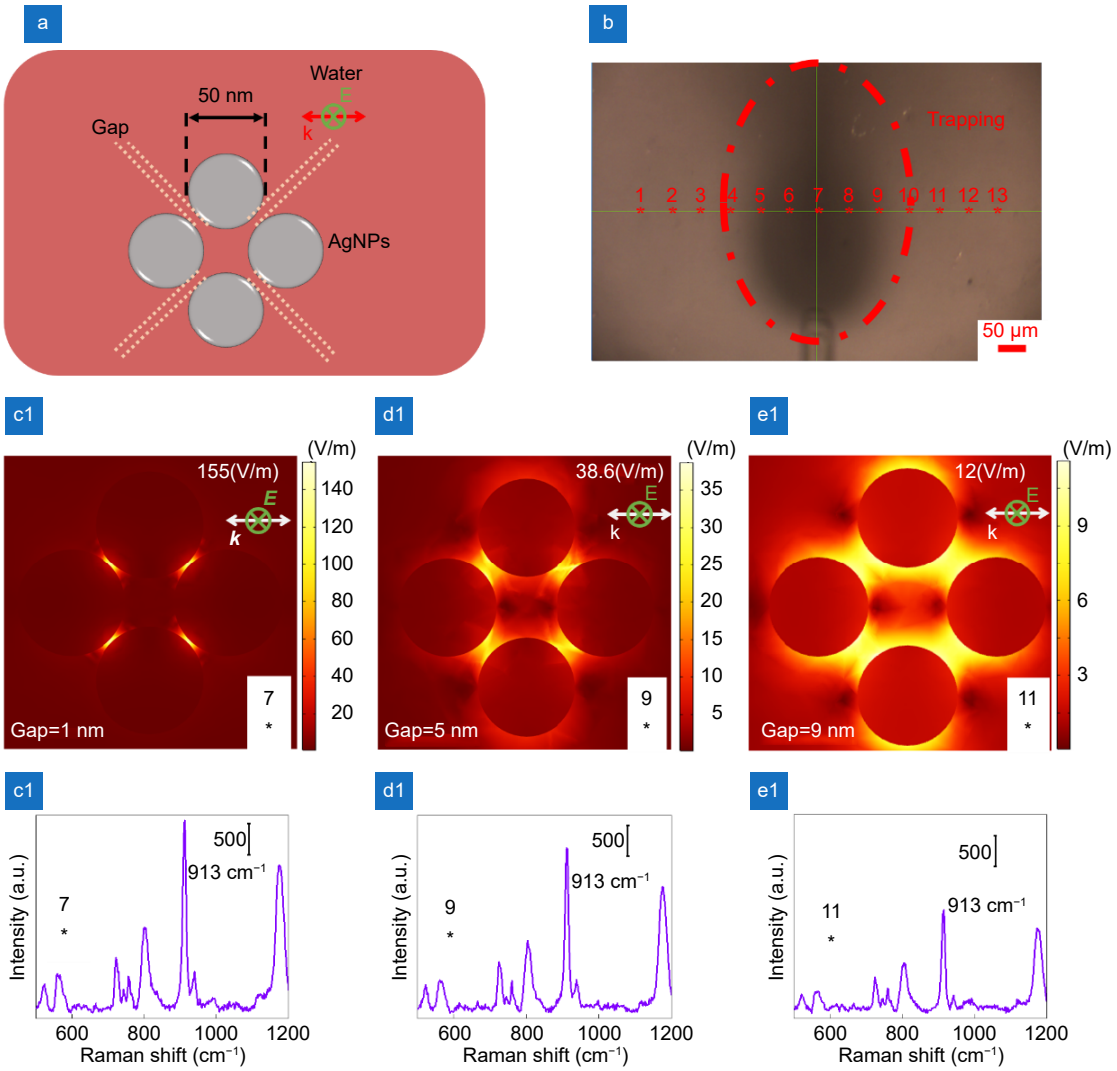

Fig. S5 | (**a**) Electric field simulation model of 50 nm diameter AgNPs under 532 nm laser excitation with different gaps. (**b**) Raman line mapping positions. (**c1**) Electric field distribution when the gap is 1 nm (position 7). (**c2**) Raman characteristic peak intensity at 913 cm^{-1} of CV at position 7. (**d1**) Electric field distribution when the gap is 5 nm (position 9). (**c2**) Raman characteristic peak intensity at 913 cm^{-1} of CV at position 9. (**e1**) Electric field distribution when the gap is 9 nm (position 11). (**c2**) Raman characteristic peak intensity at 913 cm^{-1} of CV at position 11.

References

S1. Xin HB, Li BJ. Targeted delivery and controllable release of nanoparticles using a defect-decorated optical nanofiber. *Opt Express* **19**, 13285–13290 (2011).

S2. Xu Y, Zhong HQ, Shi M et al. Microfiber-directed reversible assembly of Au nanoparticles for SERS detection of pollutants. *Opt Lett* **47**, 2028–2031 (2022).

S3. Xin HB, Li XM, Li BJ. Massive photothermal trapping and migration of particles by a tapered optical fiber. *Opt Express* **19**, 17065–17074 (2011).

S4. Daimon M, Masumura A. Measurement of the refractive index of distilled water from the near-infrared region to the ultraviolet region. *Appl Opt* **46**, 3811–3820 (2007).

S5. Rakić AD, Djurišić AB, Elazar JM et al. Optical properties of metallic films for vertical-cavity optoelectronic devices. *Appl Opt* **37**, 5271–5283 (1998).